LETTER

doi:10.1038/nature10550

A Pluto-like radius and a high albedo for the dwarf planet Eris from an occultation

B. Sicardy[1,2,3], J. L. Ortiz[4], M. Assafin[5], E. Jehin[6], A. Maury[7], E. Lellouch[1], R. Gil Hutton[8], F. Braga-Ribas[1,9], F. Colas[10], D. Hestroffer[10], J. Lecacheux[1], F. Roques[1], P. Santos-Sanz[1], T. Widemann[1], N. Morales[4], R. Duffard[4], A. Thirouin[4], A. J. Castro-Tirado[4], M. Jelínek[4], P. Kubánek[4], A. Sota[4], R. Sánchez-Ramírez[4], A. H. Andrei[5,9], J. I. B. Camargo[5,9], D. N. da Silva Neto[9,11], A. Ramos Gomes Jr[5], R. Vieira Martins[5,9,10], M. Gillon[6], J. Manfroid[6], G. P. Tozzi[12], C. Harlingten[13], S. Saravia[7], R. Behrend[14], S. Mottola[15], E. García Melendo[16,17], V. Peris[18], J. Fabregat[18], J. M. Madiedo[19], L. Cuesta[20], M. T. Eibe[20], A. Ullán[20], F. Organero[21], S. Pastor[22], J. A. de los Reyes[22], S. Pedraz[23], A. Castro[24], I. de la Cueva[25], G. Muler[26], I. A. Steele[27], M. Cebrián[28], P. Montañés-Rodríguez[28], A. Oscoz[28], D. Weaver[29], C. Jacques[30], W. J. B. Corradi[31], F. P. Santos[31], W. Reis[31], A. Milone[32], M. Emilio[33], L. Gutiérrez[34], R. Vázquez[34] & H. Hernández-Toledo[35]

The dwarf planet Eris is a trans-Neptunian object with an orbital eccentricity of 0.44, an inclination of 44 degrees and a surface composition very similar to that of Pluto[1]. It resides at present at 95.7 astronomical units (1 AU is the Earth-Sun distance) from Earth, near its aphelion and more than three times farther than Pluto. Owing to this great distance, measuring its size or detecting a putative atmosphere is difficult. Here we report the observation of a multi-chord stellar occultation by Eris on 6 November 2010 UT. The event is consistent with a spherical shape for Eris, with radius 1,163 ± 6 kilometres, density 2.52 ± 0.05 grams per cm^3 and a high visible geometric albedo, $p_V = 0.96^{+0.09}_{-0.04}$. No nitrogen, argon or methane atmospheres are detected with surface pressure larger than ~1 nanobar, about 10,000 times more tenuous than Pluto's present atmosphere[2–5]. As Pluto's radius is estimated[3–8] to be between 1,150 and 1,200 kilometres, Eris appears as a Pluto twin, with a bright surface possibly caused by a collapsed atmosphere, owing to its cold environment. We anticipate that this atmosphere may periodically sublimate as Eris approaches its perihelion, at 37.8 astronomical units from the Sun.

The dwarf planet (136199) Eris was discovered[9] in 2005. Its radius has been estimated to be 1,200 ± 100 km on the basis of direct imaging[10], although detection of its thermal flux provided another estimate[11] of 1,500 ± 200 km, potentially making it larger even than Pluto, and the largest known dwarf planet. The motion of Dysnomia (Eris' satellite) provides Eris' mass, $M_E = (1.66 \pm 0.02) \times 10^{22}$ kg, 27% larger than Pluto's mass[12]. No short-term (day-scale) brightness variability has been detected for Eris at the 1% level[13,14], suggesting either a spherical body with no albedo variegation, or—if elongated—a finely-tuned, pole-on viewing geometry. The spectrum of Eris is very similar to that of Pluto and reveals a methane-ice-rich cover, and another dominant ice, presumably nitrogen, but not excluding argon[1].

Stellar occultations by Eris are rare, as it subtends a minuscule angular diameter (~0.03 arcsec) while currently moving in severely depleted stellar fields at an angular rate of ~1.5 arcsec h^{-1} at most. Using the techniques described in ref. 15, we predicted one Eris occultation in 2010, on November 6 UT. We attempted observations from 26 stations, and the occultation was detected from two sites in Chile, with two detections at San Pedro de Atacama (San Pedro for short) with the Harlingten and ASH2 telescopes, 20 m from each other, and one detection at La Silla, with the TRAPPIST telescope (for details, see Fig. 1, Supplementary Figs 1 and 2, and Supplementary Tables 1 and 2). Another station further south at Complejo Astronómico El Leoncito (CASLEO), Argentina, provided a light curve without occultation, but went close to Eris' shadow edge (~200 km; see Fig. 2).

The San Pedro and La Silla observations provide two occultation segments—or 'chords'—whose four extremities are used to constrain Eris' size (red segments in Fig. 2). When deriving the occultation times, it appeared that two equally satisfactory solutions for the star reappearance time at the Harlingten telescope in San Pedro are possible, yielding two different chord lengths. These two solutions are separated by 1.2 s, and are respectively called solution 1 and solution 2, in chronological order. This ambiguity is due to the fact that the star reappearance occurred during a gap between consecutive exposures, corresponding to a net loss of information. The ASH2 data collected next to Harlingten did not provide enough signal-to-noise ratio to discriminate between these two solutions, and are not used in the fit described below (see Supplementary Information). As a dwarf planet, Eris is expected to be in hydrostatic equilibrium under gravity and centrifugal forces. The most general apparent limb shape is then an ellipse with semi-axes $a' > b'$ with effective radius $R_E = \sqrt{a'b'}$, defined as the radius of a disk that has the same apparent surface area as the actual body. This shape stems either from an oblate Maclaurin spheroid

[1]LESIA-Observatoire de Paris, CNRS, Université Pierre et Marie Curie, Université Paris-Diderot, 11, Rue Marcelin Berthelot, 92195 Meudon cedex, France. [2]Université Pierre et Marie Curie, 4, Place Jussieu, 75252 Paris cedex 5, France. [3]Institut Universitaire de France, 103, Boulevard Saint Michel, 75005 Paris, France. [4]Instituto de Astrofísica de Andalucía, CSIC, Apartado 3004, 18080 Granada, Spain. [5]Observatório do Valongo/UFRJ, Ladeira Pedro Antonio 43, CEP 20.080-090 Rio de Janeiro, RJ, Brazil. [6]Institut d'Astrophysique de l'Université de Liège, Allée du 6 Août 17, B-4000 Liège, Belgium. [7]San Pedro de Atacama Celestial Explorations, Casilla 21, San Pedro de Atacama, Chile. [8]Complejo Astronómico El Leoncito (CASLEO) and San Juan National University, Avenida España 1512 sur, J5402DSP, San Juan, Argentina. [9]Observatório Nacional/MCT, Rua General José Cristino 77, CEP 20921-400 Rio de Janeiro, RJ, Brazil. [10]IMCCE-Observatoire de Paris, CNRS, Université Pierre et Marie Curie, Université Lille 1, 77 Avenue Denfert-Rochereau, 75014 Paris, France. [11]Centro Universitário Estadual da Zona Oeste, Avenida Manual Caldeira de Alvarenga 1203, CEP, 23.070-200 Rio de Janeiro, RJ, Brazil. [12]INAF, Osservatorio Astrofisico di Arcetri, Largo E. Fermi 5, I-50125 Firenze, Italy. [13]Caisey Harlingten Observatory, The Grange, Scarrow Beck Road, Erpingham, Norfolk NR11 7QX, UK. [14]Observatoire de Genève, CH-1290 Sauverny, Switzerland. [15]DLR – German Aerospace Center, Rutherfordstrasse 2, 12489 Berlin, Germany. [16]Fundació Privada Observatori Esteve Duran, 08553 Seva, Spain. [17]Institut de Ciències de l'Espai (CSIC-IEEC), Facultat de Ciències, Torre C5, 08193 Bellaterra, Spain. [18]Observatori Astronòmic, Universitat de València, Calle Catedràtic José Beltrán 2, 46980 Paterna, Spain. [19]Universidad de Huelva, Facultad de Ciencias Experimentales, Avenida de las Fuerzas Armadas S/N, 21071 Huelva, Spain. [20]Centro de Astrobiología (CSIC-INTA), Carretera de Ajalvir, km 4, 28850 Torrejón de Ardoz, Madrid, Spain. [21]Observatorio astronómico de La Hita, 45840 La Puebla de Almoradiel (Toledo), Spain. [22]Observatorio de la Murta, 30153 Murcia, Spain. [23]Calar Alto Observatory, Centro Astronómico Hispano Alemán, Calle Jesús Durbán Remón, 2, 04004 Almería, Spain. [24]Sociedad Malagueña de Astronomía, Centro Cultural José María Gutiérrez Romero, Calle República Argentina 9, 29016 Málaga, Spain. [25]Astroimagen, Abad y Lasierra 58Bis, 07800 Ibiza, Spain. [26]Observatorio Nazaret, 35539 Nazaret, Lanzarote, Spain. [27]Liverpool JMU, Twelve Quays House, Egerton Wharf, Birkenhead CH41 1LD, UK. [28]Instituto de Astrofísica de Canarias, Vía Láctea s/n, 38205 La Laguna, Tenerife, Spain. [29]Observatório Astronomico Christus, Colégio Christus, Rua João Carvalho 630, Aldeota, CEP 60140140, Fortaleza, CE, Brazil. [30]Observatório CEAMIG-REA, CEP31545-120, Belo Horizonte, MG, Brazil. [31]Departamento de Física – Instituto de Ciências Exatas – Universidade Federal de Minas Gerais, Avenida Antônio Carlos 6627, 31270-901 Belo Horizonte, MG, Brazil. [32]Instituto Nacional de Pesquisas Espaciais (INPE-MCT), Divisão de Astrofísica, Avenida dos Astronautas, 1758, São José dos Campos, 12227-010, SP, Brazil. [33]Universidade Estadual de Ponta Grossa, O.A. – DEGEO, Avenida Carlos Cavalcanti 4748, Ponta Grossa 84030-900, PR, Brazil. [34]Instituto de Astronomía, Universidad Nacional Autónoma de México, Carretera Tijuana-Ensenada, km 103, 22860 Ensenada, BC, Mexico. [35]Instituto de Astronomía, Universidad Nacional Autónoma de México, Apartado Postal 70-264, 04510 México DF, Mexico.

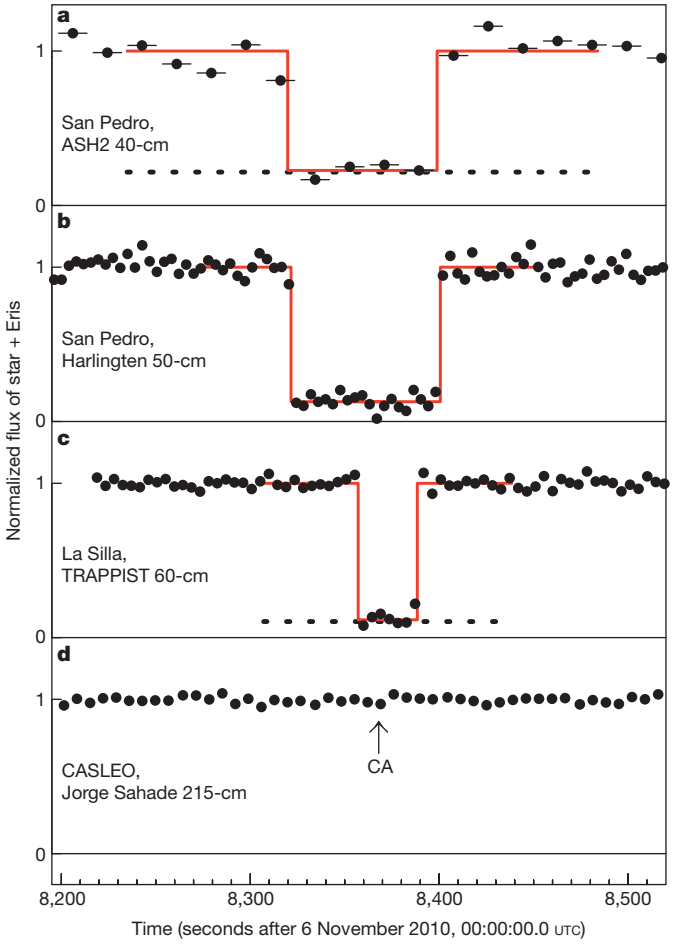

Figure 1 | Eris occultation light curves. The plots (black filled circles) show the flux of the star plus Eris, normalized to unity outside the occultation, versus time. No filter was used at any of the telescopes. **a**, The light curve from the ASH2 40-cm telescope at San Pedro, using a SBIG STL-11000M CCD camera, with 2×2 pixel binning and a sub-frame of 11.24×9.71 arcmin (272×235 pixels). The horizontal error bars indicate the total time intervals associated with each point (15 s, while the cycle time was 18.32 s). Those bars are too small to be visible on the other data sets. **b**, The light curve from the Harlingten 50-cm telescope at San Pedro using an Apogee U42 CCD camera (2×2 pixel binning; sub-frame, 2.67×2.67 arcmin, or 100×100 pixels; integration/cycle times, 3 and 3.88 s). **c**, The light curve from the 60-cm TRAPPIST telescope at La Silla, using a FLI ProLine PL3041-BB CCD camera (2×2 pixel binning; sub-frame, 3.25×3.25 arcmin, or 150×150 pixels; integration/cycle times, 3 and 4.55 s). **d**, The light curve from the 215-cm Jorge Sahade telescope at CASLEO, using a Roper Scientific Versarray 1300B CCD camera (3×3 pixel binning; sub-frame, 2.62×3.50 arcmin, or 77×103 pixels; integration/cycle times, 4 and 7 s). The horizontal dashed lines at the bottom of **a** and **c** represent Eris' contribution to the flux, showing that the star completely disappeared during the event (Supplementary Information, section 2). The red lines are the best square-well models fitted to the events. We show in **b** solution 2 for the light curve (solution 1 being very close at that scale, Supplementary Fig. 3). The vertical arrow in **d** shows the time of closest approach (CA) to the shadow edge at CASLEO, at 8,368 s UT.

(small angular momentum regime) with assumed equator-on viewing, or an elongated triaxial Jacobi ellipsoid (large angular momentum regime) observed pole-on, as implied by the absence of brightness variations.

We have five free parameters to adjust: a', the apparent flattening $(a'-b')/a'$, the ellipse position angle P in the sky plane, and the two coordinates of its centre, f_c, g_c (Supplementary Table 3). With four chord extremities, our observations allow for an infinity of limb solutions. However, as the two chords have almost the same median lines (Fig. 2), this strongly suggests that Eris' shape is indeed close to spherical,

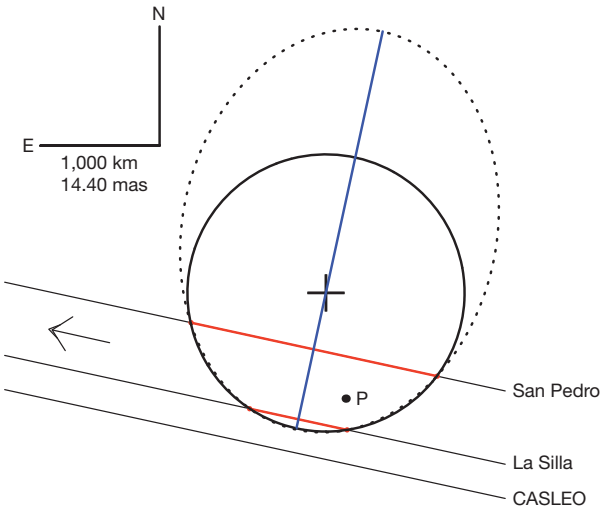

Figure 2 | Measuring Eris' size. The three oblique solid lines show the star trajectories relative to Eris, as seen from San Pedro, La Silla and CASLEO, with the arrow pointing towards the direction of motion. The San Pedro and La Silla timings provide the lengths of the two occultation segments, or 'chords' (in red); see solution 2 in Supplementary Table 3. The median lines of the two red segments are separated by only 5 km and coincide at that scale with the blue line. Celestial north is up and east is left. Scale bars: 1,000 km and 14.40 mas (1 mas corresponds to 69.436 km at Eris). The solid circle has a radius $R_E = 1{,}163$ km, and is our preferred solution for Eris' size and shape, with the cross marking the position of the centre. The dot near 'P' indicates Dysnomia's orbit pole direction[12] projected onto Eris' surface. The dotted curve is an elliptic limb fitted to our occultation chords, with semi-major and -minor axes of $a' = 1{,}708$ and $b' = 1{,}317$ km, respectively, that is, an apparent effective radius of $R_E = 1{,}500$ km, the value of Eris' radius previously derived from thermal measurements[11]. The long axis of the ellipse should be perpendicular to the occultation chords to within $\pm 2^\circ$ in order to match our data points. This has a low probability (2%) of occurring for a random limb orientation between 0 and 180°. Furthermore, the ellipse has an aspect ratio $b/a = 0.771$ that would require a fast rotator (with a period of 4.4 h) observed pole-on to within 18° to suppress the rotational light curve[13,14]. This has also a low probability (5%) of occurring for a randomly distributed pole orientation, making the dotted limb solution unlikely.

unless very special geometries occurred (see below). Using a circular model with three free parameters ($R_E = a', f_c, g_c$) and adopting solution 2, we obtain $R_E = 1{,}163 \pm 6$ km (1σ formal error). The minimum χ^2 per degree of freedom, $\chi^2_{pdf} = 1.38$, indicates a satisfactory fit to the data (Supplementary Table 3). Moreover, the r.m.s. radial residual of 2.1 km is fully consistent with our formal timing errors. We may not exclude, however, the possibility that random topographic features with amplitude approximately ±3 km exist along the limb, which would result in a slightly larger error bar for Eris' radius, $R_E = 1{,}163 \pm 9$ km (see Supplementary Information). Solution 1 provides $R_E = 1{,}140$ km, but with a high value $\chi^2_{pdf} = 30.7$ (5.5σ level), and radial residuals of +11 km and −16 km at the beginning and end of the San Pedro chord, respectively. Topographic features of this size are unlikely on such a large icy body. This indicates that the spherical assumption is not correct for solution 1, and explains why we do not provide a formal error bar for that value.

Allowing for a non-zero flattening of Eris' limb, we find an infinity of possible solutions by fixing the position angle P and semi-major axis a' at various values. If Eris' rotation axis and Dysnomia's orbital pole are aligned, we find values of R_E in the range 1,105–1,155 km, smaller than the value 1,163 km derived above. Relaxing the constraint on Eris' orientation, we find that elliptical limb models can satisfactorily fit the occultation chords in 68.3% of the cases (1σ level) for R_E in the range $1{,}165 \pm 90$ km (Supplementary Fig. 4). However, as R_E departs from 1,165 km, the flattening must rapidly increase, requiring fast rotations which are not supported by observations[13,14]. The extreme case of

$R_E = 1{,}500$ km previously found[11] can be ruled out, as it requires fine tunings in both Eris' limb and pole orientations (Fig. 2). Thus, the most straightforward interpretation of our observations is that Eris is close to spherical, remembering that larger sizes are possible in a narrow region of the parameter space. Consequently, Eris is close in size to Pluto, whose radius[3–8] is estimated between 1,150 and 1,200 km.

Our radius value implies a density of $\rho = 2.52 \pm 0.05\,\mathrm{g\,cm^{-3}}$, when combined with Eris' mass[12]. This is comparable to Haumea's density[16,17] ($\sim 2.6\,\mathrm{g\,cm^{-3}}$), for which a typical rock/ice ratio of 0.85/0.15 is derived[18]. This suggests that Haumea (and thus also Eris) is a large rocky body with a thin overlying ice shell. Note that the densities of trans-Neptunian objects (TNOs) span a large range, with ρ values of 1.0, 1.6 and $2.0\,\mathrm{g\,cm^{-3}}$ for Varuna[17], Charon[19] and Pluto[19], respectively, pointing to diverse origins and/or evolutions. Our radius value provides a geometric albedo of $p_V = 0.96^{+0.09}_{-0.04}$ in the visible range (Supplementary Information). This makes Eris almost as bright as a perfect isotropic Lambert surface (for which $p_V = 1$ by definition), and one of the intrinsically brightest objects of the Solar System. For comparison, Saturn's satellite Enceladus is even brighter, with a geometric albedo of $p_V \approx 1.4$, associated with its geologically active surface[20]. In contrast, Eris' brightness and lack of light-curve variations may stem from the collapse of a nitrogen atmosphere (see below). We find that Eris is brighter than the TNO 2002 TX_{300}, whose high albedo ($0.88^{+0.15}_{-0.06}$) is probably due to the exposure of fresh water-ice[21].

We now reassess Eris' surface temperature in the light of our new results. Measurements by the Spitzer[22] and IRAM[11] satellites imply disk-averaged brightness temperatures of $T_b = 30 \pm 1.2$ K and $T_b = 38 \pm 7.5$ K at 70 and 1,200 μm, respectively. As a completely absorbing surface at Eris' distance has a temperature $T_0 = 40$ K, the second value is surprisingly high (and consistent with the fact that the previously found radius[11] of 1,500 km is about 30% higher than our value), but we note that a unique brightness temperature $T_b \approx 31$ K matches both the Spitzer (at 70 μm) and IRAM (1,200 μm) measurements at the 1.5σ level (Supplementary Fig. 5). However, Eris' surface temperature is probably not uniform, because an atmosphere (if any) would be too tenuous to isothermalize the surface frosts, as occurs for Triton and Pluto. We therefore consider two extreme standard temperature distribution models, corresponding to (1) a warmer slow rotator (or equivalently, pole-on orientation, or zero thermal inertia, the standard thermal model, STM) with sub-solar temperature T_{ss}, and (2) a cooler fast rotator with equator-on geometry (isothermal with latitude model, ILM), with equatorial temperature T_{eq}.

In the STM, both Spitzer and IRAM fluxes are reproduced satisfactorily with $T_{ss} \approx 35$ K (Supplementary Fig. 5, Supplementary Tables 4 and 5). The thermal equilibrium equation $T_{ss} = T_0[(1 - p_V q)/(\varepsilon\eta)]^{1/4}$ then provides a relationship between the beaming factor η (describing the effects of surface roughness), the phase integral q and the surface emissivity ε, where $A = p_V q$ is the Bond albedo, which measures the fraction of reflected solar energy. Using a standard value[22] $\varepsilon = 0.9$ and a plausible range from $\eta = 1$ (no roughness) to 0.7 (large surface roughness), we obtain $q = 0.49$–0.66, fully consistent with the values for Saturn's brightest icy satellites[20,23]. The ILM in contrast leads to the extreme condition $0 < q < 0.24$, which is an implausible range as bright objects also have large phase integrals[24]. Essentially, the fast rotator model does not provide enough thermal flux given the new, smaller size of Eris. We therefore strongly favour the STM, implying either a pole-on orientation or a very small thermal inertia, as observed in other TNOs[25,26].

The occultation puts an upper limit on a putative atmosphere around Eris. As discussed in Supplementary Information, our preferred model is an isothermal N_2 atmosphere near 30 K, for which we can place an upper limit of about 1 nbar (1σ level) at the surface (Fig. 3). Similar limits are obtained for hypothetical CH_4 or Ar atmospheres. Also discussed in Supplementary Information is the possibility that a Pluto-like atmosphere sublimates as Eris approaches its perihelion, at 37.8 AU from the Sun. In that case, Eris would currently be a dormant Pluto twin, with a bright icy surface created by a collapsed atmosphere. Detailed models are required, however, to confirm this model.

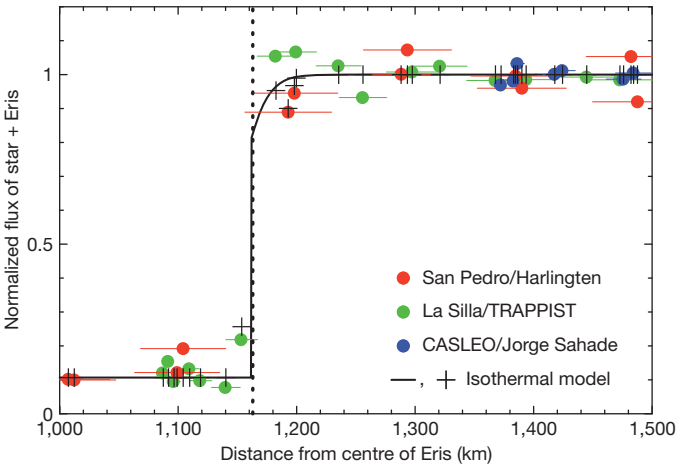

Figure 3 | Upper limit on Eris' atmosphere. Each data point (filled coloured circles) obtained at three of the stations shown in Fig. 2 has been projected onto a radial scale (distance from Eris' centre), using the circular solution 2 displayed in Fig. 2. The horizontal bars indicate the finite radial resolution associated with finite integration intervals; the vertical dotted line shows the adopted Eris radius, $R_E = 1{,}163$ km. The black solid line is a model light curve obtained at 1-km resolution, using an isothermal pure N_2 atmosphere. Black crosses mark the expected flux associated with each data point, once the convolution with the finite integration intervals has been performed. The fit minimizes the differences between the black crosses and the corresponding data points (filled circles). The model shown here is the 3σ-level upper limit of an isothermal N_2 atmospheric profile, with $T = 27.7$ K and a surface pressure of 2.9 nbar. Most of the constraint on the model comes from the two data points obtained at La Silla (the two green filled circles just right of the vertical dotted line), corresponding to the data points obtained just before and just after the event (Fig. 1). The two closest San Pedro data points (red) have only a small contribution to the χ^2 value, while the CASLEO data points (blue) are too far away from Eris' edge ($\sim$200 km) to effectively constrain the atmospheric pressure. Using solution 1 instead of solution 2 for Eris' shape would have a minimal impact on the atmospheric upper limit, as this would slightly displace the San Pedro data points in the plot, leaving the La Silla points where they are shown here.

Received 5 June; accepted 6 September 2011.

1. Tegler, S. C. *et al.* Methane and nitrogen abundances on Pluto and Eris. *Astrophys. J.* **725,** 1296–1305 (2010).
2. Yelle, R. V. & Elliot, J. L. in *Pluto and Charon* (eds Stern, S. A. & Tholen, D. J.) 347–390 (Univ. Arizona Press, 1997).
3. Elliot, J. L. *et al.* Changes in Pluto's atmosphere: 1988–2006. *Astron. J.* **134,** 1–13 (2007).
4. Lellouch, E. *et al.* Pluto's lower atmosphere structure and methane abundance from high-resolution spectroscopy and stellar occultations. *Astron. Astrophys.* **495,** L17–L21 (2009).
5. Zalucha, M. A. *et al.* An analysis of Pluto occultation light curves using an atmospheric radiative–conductive model. *Icarus* **211,** 804–818 (2011).
6. Tholen, D. J. & Buie, M. W. Further analysis of Pluto-Charon mutual event observations. *Bull. Am. Astron. Soc.* **22,** 1129 (1990).
7. Young, E. F. & Binzel, R. P. A new determination of radii and limb parameters for Pluto and Charon from mutual event lightcurves. *Icarus* **108,** 186–199 (1994).
8. Tholen, D. J. & Buie, M. W. in *Pluto and Charon* (eds Stern, S.A. & Tholen, D.J.) 193–219 (Univ. Arizona Press, 1997).
9. Brown, M. E., Trujillo, C. A. & Rabinowitz, D. L. Discovery of a planetary-sized object in the scattered Kuiper Belt. *Astrophys. J.* **635,** L97–L100 (2005).
10. Brown, M. E., Schaller, E. L., Roe, H. G., Rabinowitz, D. L. & Trujillo, C. A. Direct measurement of the size of 2003 UB313 from the Hubble Space Telescope. *Astrophys. J.* **643,** L61–L63 (2006).
11. Bertoldi, F. F. Altenhoff, W. Weiss, A., Menten, K. M. & Thum, C. The trans-neptunian object UB_{313} is larger than Pluto. *Nature* **439,** 563–564 (2006).
12. Brown, M. E. & Schaller, E. L. The mass of dwarf planet Eris. *Science* **316,** 1585 (2007).
13. Sheppard, S. S. *et al.* Light curves of dwarf plutonian planets and other large Kuiper Belt Objects: their rotations, phase functions, and absolute magnitudes. *Astron. J.* **134,** 787–798 (2007).
14. Duffard, R. *et al.* A study of photometric variations on the dwarf planet (136199) Eris. *Astron. Astrophys.* **479,** 877–881 (2008).

15. Assafin, M. *et al.* Precise predictions of stellar occultations by Pluto, Charon, Nix and Hydra for 2008–2015. *Astron. Astrophys.* **515,** A32 (2010).
16. Rabinowitz, M. E. *et al.* Photometric observations constraining the size, shape, and albedo of 2003 EL61, a rapidly rotating, Pluto-sized object in the Kuiper Belt. *Astrophys. J.* **639,** 1238–1251 (2006).
17. Lacerda, P. & Jewitt, D. C. Densities of solar system objects from their rotational light curves. *Astron. J.* **133,** 1393–1408 (2007).
18. McKinnon, W. B., Prialnik, D., Stern, S. A. & Coradini, A. in *The Solar System Beyond Neptune* (eds Barucci, M. A., Boehnhardt, H., Cruikshank, D. P. & Morbidelli, A.) 213–241 (Univ. Arizona Press, 2008).
19. Tholen, D. J., Buie, M. W., Grundy, W. M. & Elliott, G. T. Masses of Nix and Hydra. *Astron. J.* **135,** 777–784 (2008).
20. Verbiscer, A., French, R., Showalter, M. & Helfenstein, P. Enceladus: cosmic graffiti artist caught in the act. *Science* **315,** 815 (2007).
21. Elliot, J. L. *et al.* Size and albedo of Kuiper belt object 55636 from a stellar occultation. *Nature* **465,** 897–900 (2010).
22. Stansberry, J. *et al.* in *The Solar System beyond Neptune* (eds Barucci, M. A., Boehnhardt, H., Cruikshank, D. P. & Morbidelli, A.) 161–179 (Univ. Arizona Press, 2008).
23. Howett, C. J. A., Spencer, J. R., Pearl, J. & Segura, M. Thermal inertia and bolometric Bond albedo values for Mimas, Enceladus, Tethys, Dione, Rhea and Iapetus as derived from Cassini/CIRS measurements. *Icarus* **206,** 573–593 (2010).
24. Brucker, M. J. *et al.* High albedos of low inclination classical Kuiper belt objects. *Icarus* **201,** 284–294 (2009).
25. Müller, T. G. *et al.* ''TNOs are cool'': a survey of the trans-Neptunian region. I. Results from the Herschel science demonstration phase (SDP). *Astron. Astrophys.* **518,** L146 (2010).
26. Lellouch, E. *et al.* ''TNOs are cool'': a survey of the trans-Neptunian region. II. The thermal lightcurve of (136108) Haumea. *Astron. Astrophys.* **518,** L147 (2010).

Supplementary Information is linked to the online version of the paper at www.nature.com/nature.

Acknowledgements We thank W. M. Owen and S. Preston for providing astrometric updates on the occulted star just before the observations, and I. Belskaya and M. E. Brown for discussions when writing the paper. We acknowledge support from the French grant 'Beyond Neptune' and from the Institut Universitaire de France. J.L.O., A.J.C.-T., L.C. and M.T.E. acknowledge funding from Spanish AYA grants and FEDER funds. TRAPPIST is a project funded by the Belgian Fund for Scientific Research (FRS-FNRS) with the participation of the Swiss National Science Foundation (SNF). J.I.B.C. acknowledges CNPq and FAPERJ grants. F.B.-R. acknowledges the support of CDFB/CAPES, Brazil. W.J.B.C., W.R. and F.P.S. thank the Brazilian Agency FAPEMIG.

Author Contributions B.S. helped plan the campaign, centralized the stellar occultation predictions, participated in the observations, analysed data, wrote and ran the diffraction, limb-fitting and ray-tracing codes, and wrote part of the paper. J.L.O. helped plan the campaign, analysed data for the prediction, participated in the observations, obtained and analysed data, and wrote part of the paper. E.L. analysed the implications of the results for the Eris thermal model, albedo constraints and putative atmospheric structure, and wrote part of the paper. M.A., F.B.-R., A.H.A., J.I.B.C., R.V.M., D.N.d.S.N. and R.B. discovered the star candidate and analysed data for the predictions. E.J. and A.M. obtained and analysed the positive occultation detection at La Silla/TRAPPIST and San Pedro/Harlingten telescopes, respectively. F.B.-R., F.C., M.G. and J.M. analysed data, D.H. calculated Dysnomia's position at the moment of occultation and wrote part of the paper. All other authors participated in the planning of the campaign and/or the observations, and the authors listed in Supplementary Table 2 were responsible for the observations. All authors were given the opportunity to review the results and comment on the manuscript.

Author Information Reprints and permissions information is available at www.nature.com/reprints. The authors declare no competing financial interests. Readers are welcome to comment on the online version of this article at www.nature.com/nature. Correspondence and requests for materials should be addressed to B.S. (bruno.sicardy@obspm.fr).